Marine Pollution Bulletin 208 (2024) 116992

Contents lists available at ScienceDirect

Marine Pollution Bulletin

journal homepage: www.elsevier.com/locate/marpolbul

Seasonal and spatial variations of dissolved inorganic nitrogen exchange between the Yellow Sea and the East China Sea and the influencing factors

Yujun Liu [a,b,1], Xinyan Mao [c,1], Jie Shi [a,b,*], Yifei Luo [d], Xinyu Guo [d], Yucheng Wang [e]

[a] Key Laboratory of Marine Environment and Ecology, College of Environmental Science and Engineering, Ocean University of China, Ministry of Education, Qingdao 266100, China
[b] Laboratory for Marine Ecology and Environmental Science, Qingdao Marine Science and Technology Center, Qingdao 266237, China
[c] College of Oceanic and Atmospheric Sciences, Ocean University of China, Qingdao 266100, China
[d] Center for Marine Environmental Studies, Ehime University, Matsuyama 790-8577, Japan
[e] Laoshan Laboratory, Qingdao 266237, China

ARTICLE INFO

Keywords:
Water exchange
Dissolved inorganic nitrogen flux
Yellow Sea
East China Sea
Physical-biogeochemical coupled model

ABSTRACT

Nutrient exchange with the East China Sea plays an important role in primary production in the Yellow Sea. Owing to lack of simultaneous observations, the spatiotemporal nutrient exchanges across the boundary between the Yellow Sea and East China Sea (Section YE) remain unclear. In this study, a three-dimensional physical-biogeochemical coupled model was used to determine the flux of dissolved inorganic nitrogen (DIN) across Section YE. The results showed that DIN was transported from the East China Sea to the Yellow Sea throughout the year and was highest in summer, accounting for 38 % of the total annual amount. Seasonal variations in the DIN flux were attributed to seasonal variations in the ocean currents across Section YE. In the Yellow Sea, the annual amount of DIN from lateral boundaries was larger than the river input and was comparable to the atmospheric deposition.

1. Introduction

The nutrient in the coastal seas can be supplied by exchanging with adjacent seas through lateral boundaries (Gómez, 2003; Onitsuka et al., 2007; Grilli et al., 2013; Ding et al., 2019; Lu et al., 2020). Globally, continental shelves receive approximately 450–600 Tg N yr^{-1} via exchange with open oceans, which is 10 times that from rivers and approximately 40 times that from atmospheric deposition (Voss et al., 2013). The Tsushima Strait is a lateral boundary of the Sea of Japan, and nutrient input through the Tsushima Strait supports >70 % of the primary production in its coastal areas (Shibano et al., 2019). The Kii Channel as an eastern boundary of the Seto Inland Sea connects it to the Pacific Ocean, and dissolved inorganic nitrogen (DIN) input into the Seto Inland Sea through the Kii Channel accounts for 15 % of the DIN at the eastern Seto Inland Sea (Kobayashi and Fujiwara, 2008).

The Yellow Sea (Fig. 1), a semi-enclosed sea between the mainland China and the Korean Peninsula, is one of the Large Marine Ecosystems in the world and an important fishery (Tang et al., 2016). The construction of marine ranches has been widely promoted in coastal areas (Li et al., 2019), and new types of salmonid fish farming have been established in the central Yellow Sea Cold Water Mass (Dong, 2019). However, various marine ecological problems have arisen, including red tides (Tang et al., 2010), green tides (Li et al., 2015; Shi et al., 2015; Wang et al., 2018), jellyfish outbreaks (Sun, 2012) and hypoxia (Shi, 2020; Zhai et al., 2021). The health and function of the Yellow Sea ecosystem depend on nutrient cycling, which is closely related to nutrient transport through lateral boundaries. The Yellow Sea has three lateral boundaries: the Bohai Strait, the Cheju Strait, and the boundary between the Yellow Sea and the East China Sea (Section YE) (Fig. 1a). Spatial and seasonal variations in the material exchange across the Bohai Strait and Cheju Strait have been quantified using both observations and models (Chang et al., 2000; Lie et al., 2000; Qi et al., 2016; Liu et al., 2021a; Shin et al., 2022).

The hydrodynamic processes in the seas adjacent to Section YE are complex (Fig. 1b), resulting in variations in water and nutrient exchange. The northward intrusion of the Yellow Sea Warm Current across

* Corresponding author at: Key Laboratory of Marine Environment and Ecology, College of Environmental Science and Engineering, Ocean University of China, Ministry of Education, Qingdao 266100, China.
E-mail address: shijie@ouc.edu.cn (J. Shi).
[1] These authors contributed equally to this work.

https://doi.org/10.1016/j.marpolbul.2024.116992
Received 29 January 2024; Received in revised form 16 August 2024; Accepted 12 September 2024
Available online 22 September 2024

the Section YE brings nutrient-rich water to the Yellow Sea. The concentrations of the DIN in the Yellow Sea Warm Current were 1.6–1.8 times higher than those in the non-Yellow Sea Warm Current area (Jin et al., 2013), and the concentrations sustained enhancement (Fu et al., 2009; Jin et al., 2013; Guo et al., 2020b). The region influenced by the Yellow Sea Warm Current is closely related to the region with a high incidence of phytoplankton blooms (Xuan et al., 2011). Moreover, the strong vertical mixing of the winter monsoon replenished the nutrients carried by the deep Yellow Sea Warm Current to the surface water, providing nutrients for subsequent spring blooms in the Yellow Sea (Jin et al., 2013). As the largest river in China, the Changjiang River enters the East China Sea and expands northeastward into the Yellow Sea under the influence of southerly winds in the summer, bringing large amounts of nutrients to the Yellow Sea (Hou et al., 2021; Liu et al., 2021b). The annual average discharge of the Changjiang River is 9×10^{11} m^3, 14.1 % of which enters Yellow Sea through the western side of the Section YE (Liu et al., 2003).

Owing to the large geographical span of Section YE, it is difficult to obtain simultaneous observations of current velocities and nutrient concentrations at high spatiotemporal resolutions. Previous studies estimated the annual amount of water exchange across Section YE to be 0.21 Sv (1 Sv = 10^6 m^3/s) (Liu et al., 2003) and 0.56 Sv (Teague et al., 2003), using box models. Qi et al. (2016) calculated seasonal variations in water exchange across Section YE using a Regional Ocean Modeling System. However, the spatial distribution of the water exchange along Section YE remains unclear. Nutrient fluxes can be estimated based on water transport and nutrient concentrations. Liu et al. (2003) and Zhao et al. (2016) calculated the annual average of nitrate fluxes to be 0.65 × 10^6 and 0.41 × 10^6 mmol/s, respectively. The annual DIN fluxes were also estimated to be 0.98 × 10^6 mmol/s based on a numerical model (Jiang et al., 2020). However, the characteristics of the seasonal variations and spatial distributions of nutrient fluxes across Section YE need to be further investigated, and the influencing factors need to be discussed.

In this study, a three-dimensional physical-biogeochemical coupled model was used to simulate seasonal variations in the hydrodynamic and ecological fields of the East China Seas, and the model results were validated by observations. Given that DIN is a representative nutrient, the spatiotemporal variations in water and DIN fluxes across Section YE were calculated. The main influencing factors were analyzed by decomposing the variances. Finally, the contribution of DIN transported into the Yellow Sea through Section YE to the DIN budget is discussed.

2. Methods

2.1. Model description

The three-dimensional model used in this study consisted of both physical and biogeochemical modules (Zhao and Guo, 2011). The physical module is based on the Princeton Ocean Model (POM) (Blumberg and Mellor, 1987; Mellor, 2003), and the biogeochemical module is based on the biological part of NORWECOM (Skogen and Søiland, 1998). The physical module provided the water temperature, current velocity and turbulent viscosity coefficient for the biogeochemical components. The biogeochemical module included three types of nutrients (DIN, dissolved inorganic phosphorus, and silicate), two groups of phytoplankton (diatoms and flagellates), and two types of detritus. Previous studies have provided detailed information on physical and biogeochemical modules (Guo et al., 2006; Zhao and Guo, 2011; Wang et al., 2019).

As shown in Fig. 1, the model domain was 117.5° E–131.5° E, 24° N–41° N, covering the Bohai Sea, Yellow Sea, East China Sea, and part of the Sea of Japan. The model had a horizontal resolution of 1/18° (~6 km) and was divided vertically into 21 sigma layers. In this study, Section YE was defined as the section connecting the Changjiang Estuary (Station A: 121.82° E, 31.91° N) to the southwest of Cheju Island (Station B: 126.15° E, 33.31° N) (line AB in Fig. 1a).

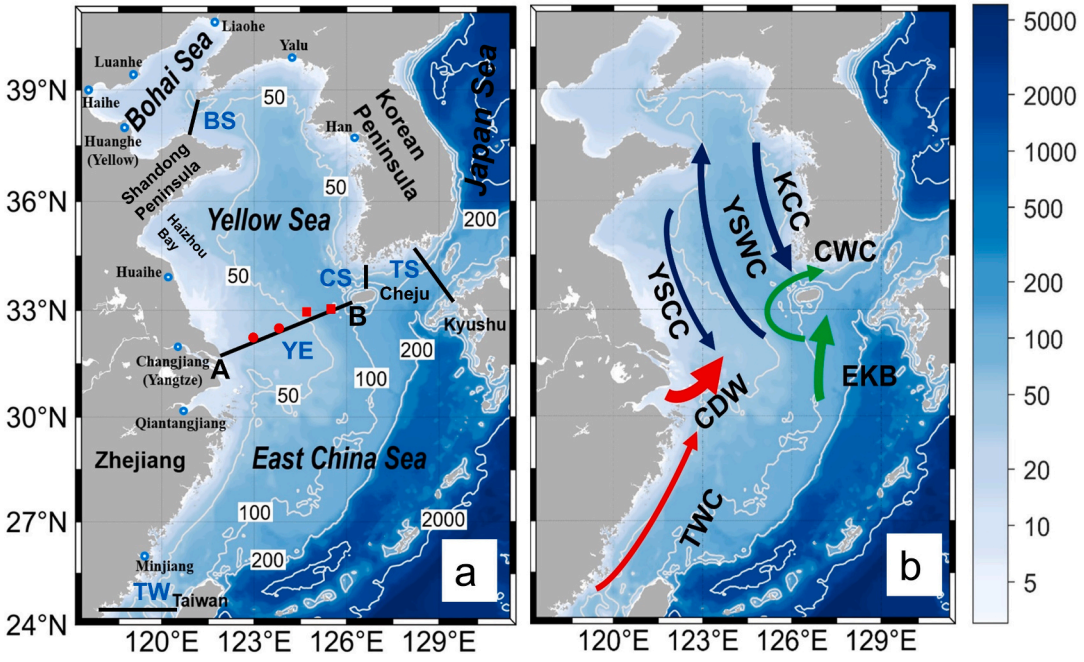

Fig. 1. (a) Map of the model domain and (b) schematic diagrams of ocean currents in southern Yellow Sea and northern East China Sea. Rivers in (a) are denoted by blue circles along the coastline. Scatters in (a) denote nutrient sampling sites in the summer and winter; red circles are the sites from Wei et al. (2016), and red squares are the sites from the National Institute of Fisheries Science (NIFS). The black lines in (a) represent sectional locations of Bohai Strait, Section YE, Cheju Strait, Tsushima Strait, and Taiwan Strait, respectively. The blue, red and green arrows in (b) represent the ocean currents in winter, summer, and all seasons, respectively. YSWC, KCC, YSCC, CDW, CWC, EKB, TWC indicate Yellow Sea Warm Current, Korean Coastal Current, Yellow Sea Coastal Current, Changjiang Diluted Water, Cheju Warm Current, Eastern Kuroshio Branch, and Taiwan Warm Current, respectively. (For interpretation of the references to color in this figure legend, the reader is referred to the web version of this article.)

2.2. Model configurations

The model reproduced climatological seasonal variations in the physical and biogeochemical variables of the East China Seas (Guo et al., 2006; Zhu et al., 2018; Wang et al., 2019; Luo et al., 2023). In this study, the initial conditions of the physical variables were derived from the stable climatological results of this model in winter (January 1) (Wang et al., 2019). The initial conditions of the three types of nutrients concentrations were obtained from the World Ocean Atlas 2005 (WOA2005) dataset, while the initial concentrations of the two groups of phytoplankton were set to a relatively small value of 0.05 mgN m^{-3}. The initial conditions of the two types of detritus were both set at 1.42×10^{-7} mgN m^{-3}, which were calculated by the death rate of the two types of phytoplankton.

Atmospheric forcing data were derived from the European Centre for Medium-Range Weather Forecasts (ECMWF; Dee et al., 2011) ERA-Interim reanalysis dataset, which included 10 m u and v wind component, sea surface pressure, evaporation rate, precipitation rate, surface net heat fluxes (short-wave and long-wave radiation, latent and sensible heat fluxes), and sea surface temperature. There were ten rivers in our model (Fig. 1a), and the monthly runoff data of the Han River was obtained from: http://www.sage.wisc.edu/riverdata, while the others were obtained from the River Sediment Bulletin of China (http://xxzx.mwr.gov.cn), published by the Ministry of Water Resources of the People's Republic of China. Monthly mean sea level, water temperature, salinity, and velocity components at the open boundaries of the model domain, were obtained from the results of an assimilative model from the Japan Coastal Ocean Predictability Experiment (JCOPE2; Miyazawa et al., 2009). The domain of JCOPE2 is 10.5° N–62°N, 108° E–180°E, covering the northwestern Pacific region. The data of atmospheric forcing, runoff of river and open boundaries conditions averaged from 1995 to 2018 were used to force the model. The riverine nutrient concentrations were obtained from previous studies, and the DIN concentration of the Changjiang River was 72.81 mmol/m^3 which was averaged from multiple observations (Zhang, 1996; Wang et al., 2002; Liu et al., 2003; 2009; Liang and Xian, 2018). The atmospheric dry and wet deposition of nutrients in the East China Seas were obtains from the observations of Zhang et al. (2011). The monthly average suspended sediment concentrations were obtained from Wang and Jiang (2008). The other forcing data were the same as those used by Wang et al. (2019).

The model was integrated for three years, and the results from the third year were used for the analysis. Winter, spring, summer, and autumn were represented as February, May, August, and November, respectively.

2.3. Observational data

To validate the model results, nutrient concentrations were observed. The DIN concentrations at 123° N and 124° N in surface, 10 m, and bottom layer along Section YE were obtained from cruise observations in July 14–August 3, 2006 and January 8–February 4, 2007 (Wei et al., 2016). The DIN concentrations at 124.7° N and 125.3° N in surface, 20 m, 50 m and bottom layer along Section YE were obtained from observations in August 17, 2007 and February 9, 2007 by the National Institute of Fisheries Science of Korea (https://www.nifs.go.kr/kodc/).

2.4. Calculation of the water volume transport and DIN flux across Section YE

The zonal (u) and meridional (v) velocities were decomposed into the velocities along Section YE (u_A) and across Section YE (u_B) according to Eq. (1). u_B was used to analyze the distributions of water volume transport in Section 3.3, and was positive when flowing into the Yellow Sea. The angle (θ) between Section YE and the east was 17.5°.

$$\begin{cases} u_A = u \cdot cos\theta + v \cdot sin\theta \\ u_B = -usin\theta + v \cdot cos\theta \end{cases} \quad (1)$$

Water volume transport (V) and DIN flux (N) were calculated using the following equations:

$$V = \iint udydz + \iint vdxdz \quad (2)$$

$$N = \iint u \cdot Cdydz + \iint v \cdot Cdxdz \quad (3)$$

where, dx is the length of the zonal grid, dy is the length of the meridional grid, dz is the depth of the sigma layer, and C is the DIN concentration.

3. Results

3.1. Seasonal variations of the current field in the southern Yellow Sea and northern East China Sea

After filtering the tidal signals, the residual currents in the southern Yellow Sea and northern East China Sea were analyzed (Fig. 2). The dynamic characteristics exhibited clear seasonal variation. In winter, strong northerly winds drove southward currents at the sea surface (Fig. 2a). The current velocities near Section YE were in the range of 5–15 cm/s. The Korean Coastal Current flowed southward along the west coast of the Korean Peninsula at a velocity of approximately 8 cm/s. One branch then turned east and flowed into the Cheju Strait together with the Cheju Warm Current, which turned clockwise around the western coast of Cheju Island. The other turned southwest, mixed with the current in the middle of the Yellow Sea and continued to flow southward to 30° N driven by the winter monsoon. In the bottom layer (Fig. 2b), the Yellow Sea Warm Current intruded northward from southwest Cheju Island into the Yellow Sea at a velocity of 8 cm/s. Moreover, its main axis lay along the west side of the Yellow Sea Trough near 123° E and split into two branches near 34° N. One branch turned northwest into Haizhou Bay, whereas the other continued to flow northward along the Yellow Sea Trough, finally reaching the vicinity of the Shandong Peninsula.

In summer, the Changjiang Diluted Water expanded northeastward and was driven by a southerly summer monsoon at the sea surface (Fig. 2c). The Changjiang Diluted Water arrived in the Cheju Strait at a velocity of approximately 25 cm/s. In the southeastern area, the Eastern Kuroshio Branch flowed into the Tsushima Strait at a velocity of up to 30 cm/s from southeastern Cheju Island and finally into the Sea of Japan. The Taiwan Warm Current was strong and reached approximately 32° N. The Yellow Sea Coast Current flowed northward along the coast of China under the influence of the summer monsoon at an average velocity of <10 cm/s. At the bottom during the summer (Fig. 2d), from 32° N–34° N, the seawater flowed westward, and the current velocities were only 1–4 cm/s. From 30° N to 32°N, an anticlockwise circulation was formed by the Eastern Kuroshio Branch, the Taiwan Warm Current, and a westerly compensation current. Southeast of the study area, the Eastern Kuroshio Branch flowed northward, and its path was similar to that at the surface. It flowed into the Tsushima Strait from southeastern Cheju Island at a velocity of approximately 15 cm/s. The seasonal variations in the current fields in the southern Yellow Sea and northern East China Sea in this study were consistent with previous research (Naimie et al., 2001; Isobe, 2008; Lie and Cho, 2016; Tak et al., 2022).

Current fields determine water volume transport. Based on the model results, the volume transports across the Tsushima and Taiwan Straits (Fig. 1) were calculated and compared with those reported in previous studies. The annual average transports across the Tsushima and Taiwan straits were estimated to be 2.67 and 1.49 Sv in our model, falling within the range of the simulated and observed values in previous studies

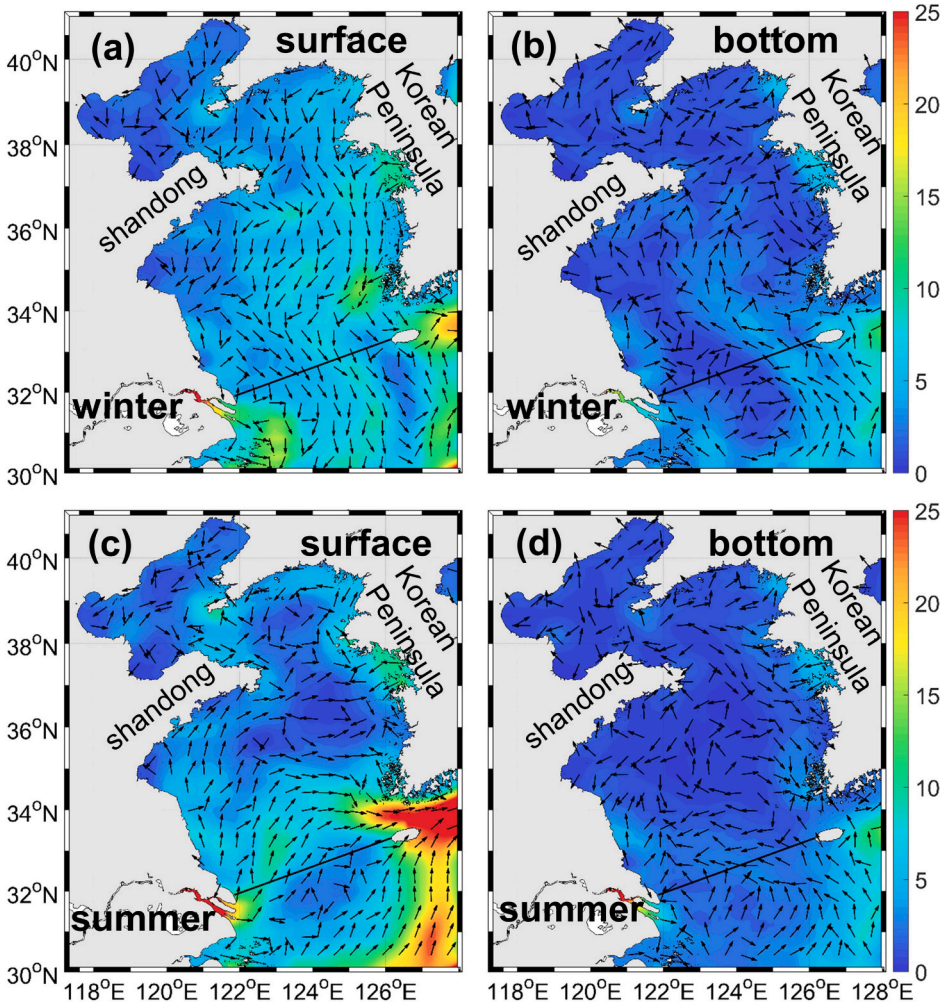

Fig. 2. Current fields (unit: cm/s) at the surface and bottom in the summer and winter. The arrows denote the current direction and the color denotes the velocity magnitude. (For interpretation of the references to color in this figure legend, the reader is referred to the web version of this article.)

Table 1
Comparisons of simulated volume transport (unit: Sv) across Taiwan Strait and the Tsushima Strait with previous studies (underscore represents observation).

	Tsushima Strait	Taiwan Strait
Teague et al. (2003)	3.17	0.14
Guo et al. (2006)	3.03	1.72
Isobe (2008)	2.65	1.20
This study	2.67	1.49

(Table 1) (Teague et al., 2003; Guo et al., 2006; Isobe, 2008). The model results also reproduced seasonal variations in volume transport across these two straits (Fig. 3) (Teague et al., 2003; Bai and Hu, 2004; Guo et al., 2006; Qi et al., 2016). The volume transport across the Tsushima Strait had a maximum value of 3.08 Sv in August and a minimum value of 2.11 Sv in February (Fig. 3a), and the volume transport across the Taiwan Strait had a maximum value of 2.16 Sv in July and a minimum value of 0.91 Sv in January, which were among the range of the published data (Fig. 3b). Because our model was driven by climatological forcing, the amplitudes of the seasonal variations were not as strong as those in previous studies, whose data were derived from a specific year.

3.2. Seasonal variations of DIN concentration along Section YE

The distributions of the model-simulated DIN concentration along Section YE overlapped with the available published observational data (Fig. 4a and c). The model results agreed well with the observations, with a correlation coefficient of 0.69 (Fig. 4e). The DIN concentrations in the southwestern part of Section YE (around the Changjiang Estuary) were high throughout the year because of the discharge of DIN from the Changjiang River. From the Changjiang Estuary to the deeper region, DIN concentrations at the sea surface decreased in all four seasons. The vertical distribution of DIN concentrations showed clear seasonal variations.

In winter (Fig. 4a), the distributions of DIN concentrations along Section YE were vertically uniform owing to the strong vertical mixing induced by both strong winter monsoons and the loss of heat from the sea surface. The DIN concentrations near the Changjiang Estuary were high, with a maximum value of over 20 mmol/m^3, and then decreased seaward to the value below 6 mmol/m^3 near southwest Cheju Island. In spring (Fig. 4b), average DIN concentration along Section YE was lower than that in winter because of absorption by phytoplankton growth. Owing to the Changjiang River input, the DIN concentrations in the southwestern region of Section YE, with water depths shallower than 40 m, were high (>10 mmol/m^3) and had a uniform vertical distribution. Stratification occurred gradually in the deeper region east of 124° E. The concentrations in the surface layer were <2 mmol/m^3 due to the vigorous growth of phytoplankton, whereas the concentrations in the deeper layers were comparably high, with values exceeding 8 mmol/m^3 due to the mineralization of organic detritus (Wei et al., 2010). In summer (Fig. 4c), the high-concentration area in the southwestern part of Section YE represents an extension of the Changjiang Diluted Water.

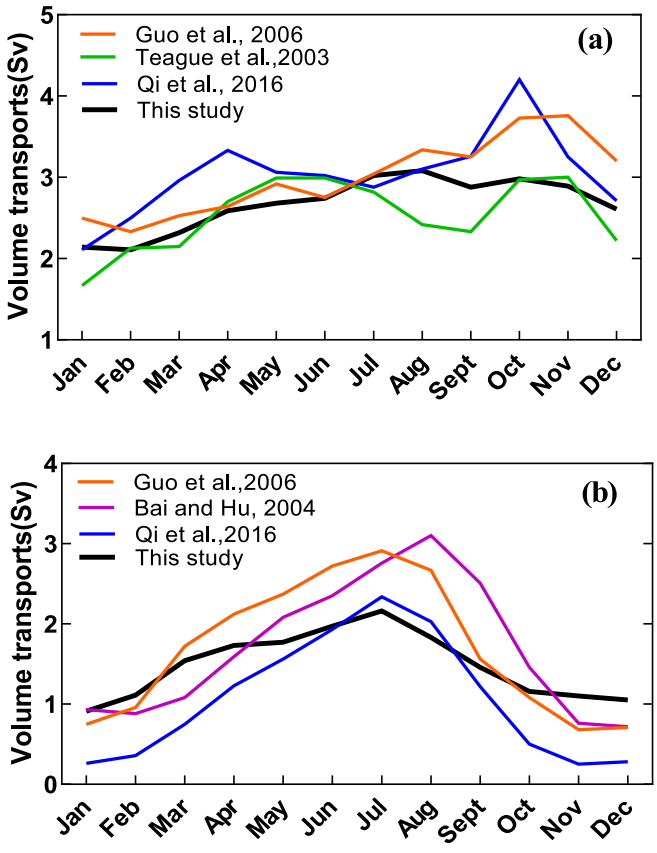

Fig. 3. Seasonal variations of volume transports (unit: Sv) across the Tsushima Strait (a) and Taiwan Strait (b).

In deeper regions, the DIN concentrations in the upper layers increased slightly, and the area with DIN concentrations lower than 2 mmol/m^3 became smaller than that in spring. This was because the growth of phytoplankton was limited by phosphate; therefore, DIN consumption decreased. However, the stratification became the strongest throughout the year because of the increase in DIN concentrations in the lower layers caused by the successive supply of mineralization (Wei et al., 2010). The concentration at the bottom of the deeper region is approximately 15 mmol/m^3. Autumn is the transitional season between the summer and winter. In the shallower region (Fig. 4d), DIN concentrations were vertically uniform, with values exceeding 8 mmol/m^3. However, stratification still existed in deeper regions. The isoline range of 4 mmol/m^3 on the surface expanded, whereas the isoline range of 10 mmol/m^3 at the bottom shrank, indicating that the nutricline gradually moved downwards towards a mixed homogeneous structure, and the water body transformed from a stratified structure in summer to a mixed homogeneous structure in winter.

3.3. Seasonal variations of water volume transport across Section YE

The monthly volume transport across Section YE was calculated from the model results and included the inflow, outflow, and net values (Fig. 5). Inflow and outflow represented the water volumes transported into and out of the Yellow Sea, respectively. The inflow had a maximum value of 0.69 Sv and a minimum value of 0.49 Sv in July and February, respectively, which was not consistent with the seasonal variations of the outflow. The peak of outflow was 0.35 Sv in November, and the minimum value of 0.19 Sv occurred in June. Throughout the year, net transport values were positive, indicating that water was transported from the East China Sea to the Yellow Sea through Section YE. The net water transport was larger in summer and weaker in winter. Both the values and seasonal variations in net transport agreed with those reported in previous studies (Qi et al., 2016).

The vertical distributions of the monthly averaged velocities across Section YE were shown in Fig. 6. Positive values represented inflow from the East China Sea to the Yellow Sea, whereas negative values represented outflow. In winter (Fig. 6a), the outflows dominated the upper 40 m of Section YE, and were induced by the northerly winter monsoon. The outflow velocity decreased with increasing depth. The inflow area occupied the lower water layers at depths deeper than 40 m in the eastern region of Section YE in all four seasons. This was caused by the Cheju Warm Current, which moved clockwise west of Cheju Island throughout the year (Chang et al., 2000; Isobe, 2008; Lie and Cho, 2016). The Cheju Warm Current extends westward, forming the Yellow Sea Warm Current as a tongue across the southern entrance of the Yellow Sea in winter (Lie and Cho, 2016). A strong inflow area at approximately 126° E from the surface to the bottom during all four seasons, with a velocity of up to 10 cm/s. This was due to the location of the core

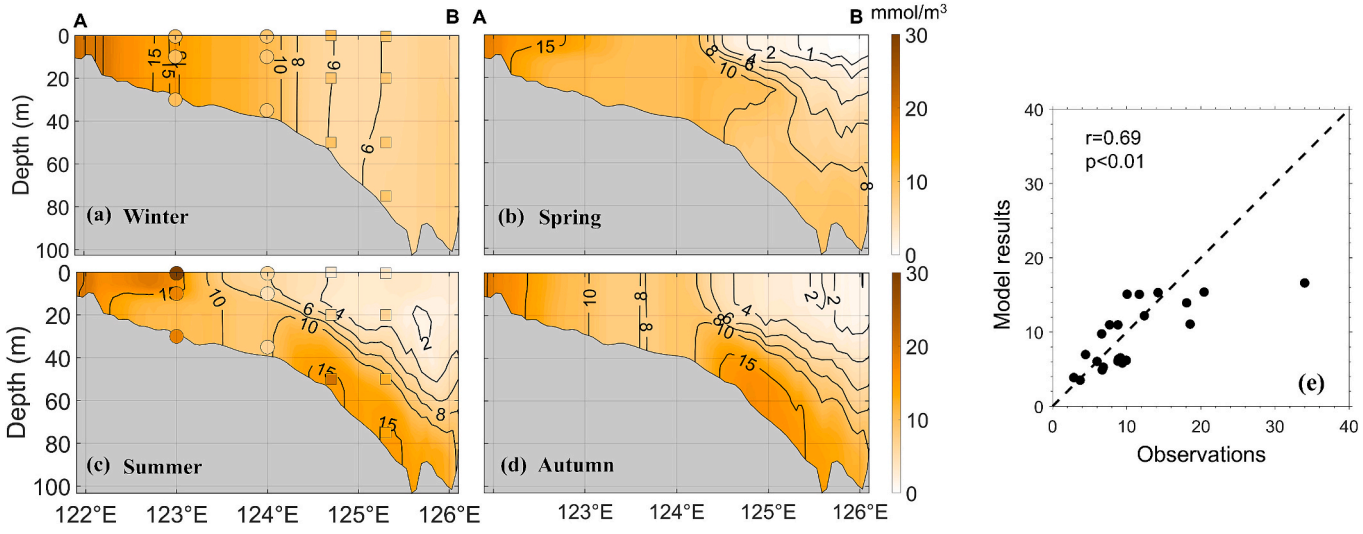

Fig. 4. Seasonal variations of DIN concentration (unit: mmol/m^3) along Section YE in winter (a), spring (b), summer (c), and autumn (d). The colored circles and squares represent the observations from Wei et al. (2016) and the National Institute of Fisheries Science (NIFS), respectively. The scatter plots of observations and corresponding model results are compared in (e). (For interpretation of the references to color in this figure legend, the reader is referred to the web version of this article.)

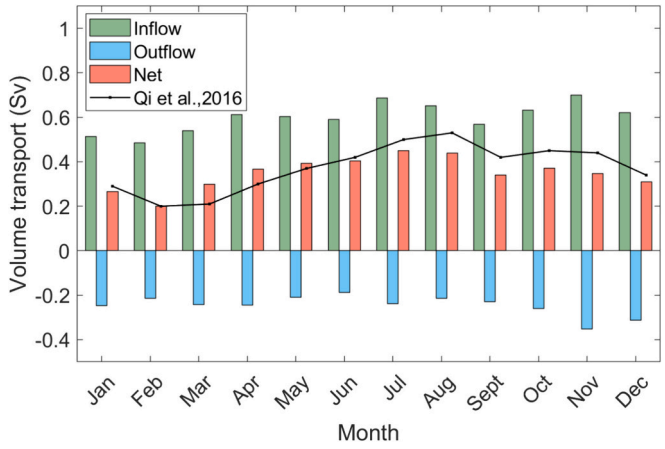

Fig. 5. Monthly mean water volume transports (unit: Sv) across Section YE. The green bars are the inflow volume transports; the blue bars are the outflow volume transports; and the red bars are the net volume transports. The positive values indicate water volume transport from the East China Sea to the Yellow Sea across Section YE, and the negative values indicate transport from the Yellow Sea to the East China Sea. (For interpretation of the references to color in this figure legend, the reader is referred to the web version of this article.)

of the Cheju Warm Current. In spring (Fig. 6b), the velocities of both the inflows and outflows weakened, which was induced by the weakening of the winter monsoon and intrusion of the Yellow Sea Warm Current. An inflow area at the sea surface west of Section YE, near the mouth of the Changjiang River. This was caused by mixing at the front of the Taiwan Warm Current and an increase in the discharge of the Changjiang Diluted Water (Chang and Isobe, 2003; Bai and Hu, 2004). In summer (Fig. 6c), the Changjiang Diluted Water expanded from the river mouth west of Cheju Island in the direction of Section YE (Hou et al., 2021). The inflows induced by the Changjiang Diluted Water were strongest near the river mouth and decreased seaward. The alternating inflows and outflows in the upper layers were determined by both the direction of extension of the Changjiang Diluted Water and the direction of Section YE. Weak inflows with velocities of <5 cm/s were still observed in the lower water layers of the middle deep region. The distribution in autumn (Fig. 6d) was similar to that in winter. In our simulations, stronger upper outflows were caused by northerly winds stronger in November than in February when averaged from 1995 to 2018. A strong inflow was induced by the Cheju Warm Current at the bottom of eastern Section YE. The onshore intrusion of the Kuroshio was strongest in autumn (Guo et al., 2006), resulting in the strongest Cheju Warm Current, which is a branch of the Kuroshio (Lie and Cho, 2016).

3.4. Seasonal variations of DIN flux across Section YE

The monthly average DIN flux across Section YE was calculated based on the model results (Fig. 7). The inflow, outflow, and net transport of DIN across Section YE exhibited clear seasonal variations. The inflow of DIN had a minimum value of 3.26×10^6 mmol/s in January, increased until summer, reaching a maximum value of 6.37×10^6 mmol/s in July, and then, decreased until the end of the year. The annual mean inflow of DIN was 4.91×10^6 mmol/s. Seasonal variations in DIN outflow differed from those in the inflow. The largest outflow of DIN occurred in winter with a value of 2.84×10^6 mmol/s in December, which was approximately twice its minimum value of 1.53×10^6 mmol/s in summer (June). Seasonal differences in DIN outflow were not as evident as those in the inflow, and the outflow was significantly weaker than the inflow. Therefore, the net transport of DIN was estimated to be the inflow into the Yellow Sea throughout the year. Net transport followed similar seasonal variations in the inflow of DIN, with a maximum value of 4.44×10^6 mmol/s in June and a minimum value of 0.95×10^6 mmol/s in January. The annual transport of DIN across the Section YE from the East China Sea to the Yellow Sea was 2.80×10^6 mmol/s. The net inflows of DIN were 3.16×10^6, 4.21×10^6, 2.54×10^6 and 1.17×10^6 mmol/s in spring (March to May), summer (June to August), autumn (September to November), and winter (December to February),

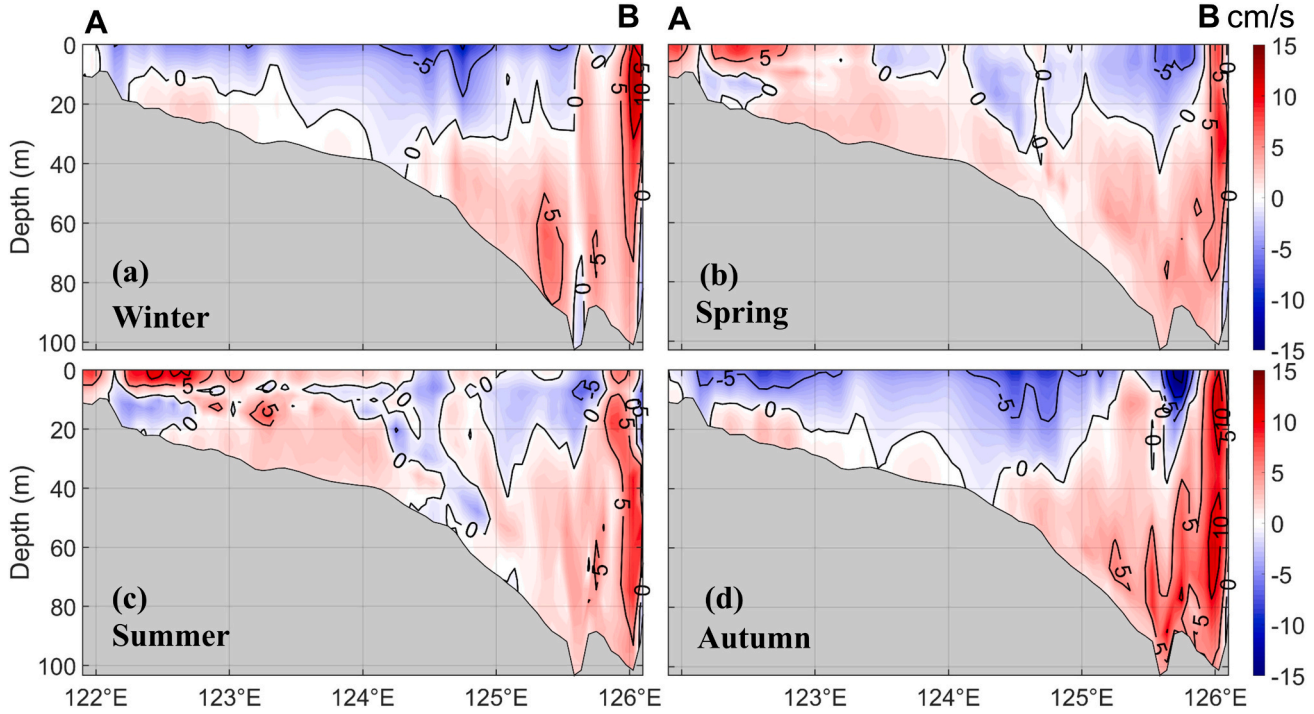

Fig. 6. Seasonal variations of velocity (unit: cm/s) across Section YE in (a) winter, (b) spring, (c) summer, and (d) autumn. Red and blue indicate inflow and outflow for the Yellow Sea through Section YE, respectively. (For interpretation of the references to color in this figure legend, the reader is referred to the web version of this article.)

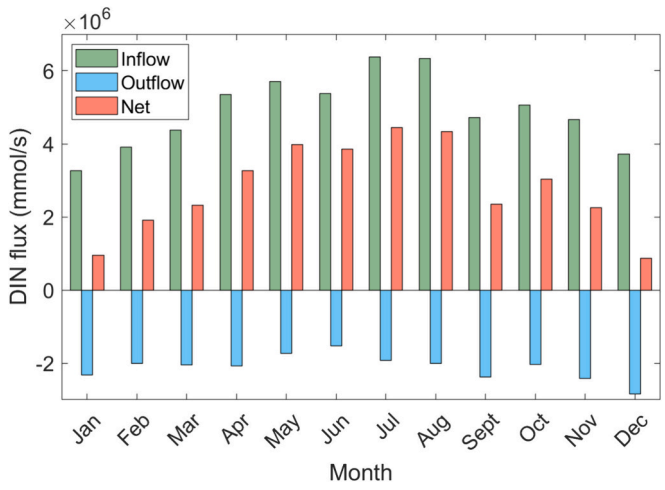

Fig. 7. Monthly mean DIN fluxes (unit: mmol/s) across Section YE. The green bars are the inflow of DIN; the blue bars are the outflow of DIN; and the red bars are the net DIN flux. The positive values indicate DIN flux transport from the East China Sea to the Yellow Sea across Section YE, and the negative values indicate that transport from the Yellow Sea to the East China Sea. (For interpretation of the references to color in this figure legend, the reader is referred to the web version of this article.)

respectively. The inflow of DIN in summer was the largest, accounting for 38 % of the total annual amount, whereas that in winter was the smallest, accounting for 10 %.

Fig. 8 shows the vertical distribution of the DIN fluxes across Section YE during the four seasons. In winter (Fig. 8a), there was an area with a strong inflow of DIN near 122°E in the southeastern coastal region of Section YE. The inflow of DIN reached 1 mmol m^{-2} s^{-1} due to the high DIN concentration near the mouth of the Changjiang River and northward coastal currents in winter. The outflows of DIN occupied the surface layer of Section YE, reached above 0.5 mmol m^{-2} s^{-1}, and were caused by a southward current triggered by northerly winds in winter. The inflow of DIN into the western part of Section YE was caused by the invasion of the Yellow Sea Warm Current. In spring (Fig. 8b), the inflow of DIN reached approximately 1 mmol m^{-2} s^{-1} in the water layers of the upper 10 m from 122° E to 123° E, which was due not only to the high DIN concentrations but also to the strong discharge of the Changjiang Diluted Water. Owing to the stratification in the eastern part of the Section YE, the DIN fluxes were low in the surface layer and high in the bottom layer. In summer (Fig. 8c), the western area of Section YE exhibited high DIN fluxes, which was a result of the further expansion of the Changjiang Diluted Water. In the eastern waters, owing to the intensification of stratification, high DIN fluxes were concentrated in the bottom layer. The inflows of DIN were approximately 0.5 mmol m^{-2} s^{-1}. Autumn is a transitional period (Fig. 8d). The outflows of DIN in the surface layers of the Section YE were similar to those in winter. The location of the 0.5 mmol m^{-2} s^{-1} isoline was similar to that in summer, however, area with high values expanded in autumn.

4. Discussions

4.1. Influencing factors of seasonal variations in DIN flux across Section YE

To discuss the influencing factors of DIN flux seasonal variations across Section YE, the variances were decomposed into six easily interpretable terms (Guo et al., 2012).

The velocity (V_i) across Section YE and DIN concentration (C_i) can be expressed as the sum of the temporal average ($\overline{V}, \overline{C}$) and anomaly value ($V_i^{'}, C_i^{'}$), which are expressed as follows:

$$\overline{C} = \frac{1}{N}\sum_{i=1}^{N} C_i, \overline{V} = \frac{1}{N}\sum_{i=1}^{N} V_i, C_i^{'} = C_i - \overline{C}, V_i^{'} = V_i - \overline{V},$$

where N is the total number of days in a year (365), and i represents the time index. Therefore, the DIN flux can be expressed as:

$$F_i = \overline{V}\overline{C} + \overline{V}C_i^{'} + V_i^{'}\overline{C} + V_i^{'}C_i^{'}, \quad (4)$$

and the temporal average of DIN flux ($\overline{F}$) is expressed as:

$$\overline{F} = \overline{V}\overline{C} + \frac{1}{N}\sum_{i=1}^{N} V_i^{'}C_i^{'} \quad (5)$$

For convenience in the following discussion, parameter G is defined as $_i = V_i^{'}C_i^{'}$; thus:

$$\overline{G} = \frac{1}{N}\sum_{i=1}^{N} V_i^{'}C_i^{'}.$$

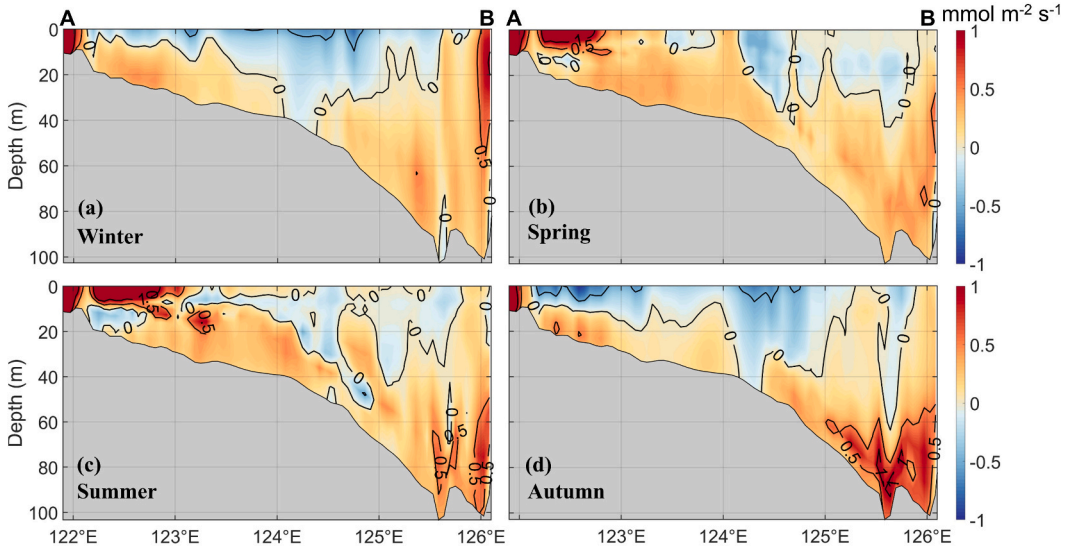

Fig. 8. Seasonal variations of DIN flux (unit: mmol m^{-2} s^{-1}) across Section YE in (a) winter, (b) spring, (c) summer, and (d) autumn. Red and blue indicate inflow and outflow for the Yellow Sea, respectively. (For interpretation of the references to color in this figure legend, the reader is referred to the web version of this article.)

Substituting this into Eq. (5), we obtain:

$$\overline{F} = \overline{V}\overline{C} + \overline{G} \tag{6}$$

The variance of DIN flux (σ_F^2) is defined as:

$$\sigma_F^2 = \frac{1}{N}\sum_{i=1}^{N}(F_i - \overline{F})^2 \tag{7}$$

Substituting Eqs. (4) and (6) into Eq. (7), we obtain:

$$\sigma_F^2 = \overline{C}^2\sigma_V^2 + \overline{V}^2\sigma_C^2 + 2\overline{C}\overline{V}\sigma_{CV}^2 + 2\overline{C}\sigma_{VG}^2 + 2\overline{V}\sigma_{CG}^2 + \sigma_G^2 \tag{8}$$

Here

$\sigma_V^2 = \frac{1}{N}\sum_{i=1}^{N}(V_i - \overline{V})^2$, $\sigma_C^2 = \frac{1}{N}\sum_{i=1}^{N}(C_i - \overline{C})^2$, $\sigma_{CV}^2 = \frac{1}{N}\sum_{i=1}^{N}(C_i - \overline{C})(V_i - \overline{V})\sigma_{VG}^2 = \frac{1}{N}\sum_{i=1}^{N}(V_i - \overline{V})(G_i - \overline{G})$, $\sigma_{CG}^2 = \frac{1}{N}\sum_{i=1}^{N}(C_i - \overline{C})(G_i - \overline{G})$, $\sigma_G^2 = \frac{1}{N}\sum_{i=1}^{N}(G_i - \overline{G})^2$.

According to Eq. (8), these six terms are associated with the variance of velocity (σ_V^2), variance of DIN concentration (σ_C^2), covariance of velocity and DIN concentration (σ_{CV}^2), covariance of velocity and $G(\sigma_{VG}^2)$, covariance of DIN concentration and $G(\sigma_{CG}^2)$, and the variance of $G(\sigma_G^2)$, respectively.

The variance of DIN flux (σ_F^2) represented temporal variations of DIN flux across Section YE. In Fig. 9a, there was an area with high values of σ_F^2 in the coastal waters west of 123° E, suggesting that the seasonal variations of DIN flux in this area were more significant. The area with σ_F^2 of approximately 1.0 mmol m^{-4} s^{-2} occupied the surface layer. The σ_F^2 values in the upper 10 m were larger than 0.2 mmol m^{-4} s^{-2}, and then decreased as the water depth increased. The higher σ_F^2 values were caused by the discharge of the Changjiang River, indicated by a high correlation coefficient of 0.73 between the DIN flux with most significant seasonal variations and the DIN discharge of the river. Another area of large σ_F^2 is found along the bottom of the deeper region east of 124°E, with σ_F^2 values exceeding 0.05 mmol m^{-4} s^{-2}. σ_F^2 values in the lower water layers of the western region and upper layers of the eastern region were <0.01 mmol m^{-4} s^{-2}, indicating more steady DIN flux across the Section YE.

To discuss the factors influencing the seasonal variations in the DIN flux across the Section YE, the six decomposed terms of σ_F^2 were calculated as defined Eq. (8) (Fig. 9b–g). $\overline{C}^2\sigma_V^2$ (about the mean nutrient concentration and the variance of velocity) was the largest of the six terms (Fig. 9b). It varied from 0to 1.56 mmol m^{-4} s^{-2}, with the same magnitude of σ_F^2. With the exception of $\overline{C}^2\sigma_V^2$, the magnitudes of the other five items were one to two orders of magnitude smaller than that of σ_F^2. This indicates that $\overline{C}^2\sigma_V^2$ was responsible for seasonal variations in the DIN flux across the Section YE. Because $\overline{C}^2$ is the annual average concentration of DIN with no seasonal variations for a given site at the Section YE, the seasonal variations in DIN flux were mainly determined by the temporal variations in current velocity denoted by σ_V^2.

The spatial distribution of the six terms differed. The distributions of $\overline{C}^2\sigma_V^2$ (Fig. 9b) are highly consistent with those of σ_F^2, suggesting that the spatial distributions of σ_F^2 were determined by $\overline{C}^2\sigma_V^2$. $\overline{V}^2\sigma_C^2$ (about the mean velocity and the variance of nutrient concentration) (Fig. 9c) had large values in the lower layers of the deeper region with a water depth exceeding 60 m and the entire water column of the eastern end of Section YE. The $2\overline{C}\overline{V}\sigma_{CV}^2$ (about the mean nutrient concentration, the mean velocity and the covariance of velocity and the nutrient concentration) value was comparably high in the surface layer (Fig. 9d). The distributions of the high values of $2\overline{C}\sigma_{VG}^2$ (about the mean nutrient concentration and the covariance of velocity and the G_i) and σ_G^2 (the variance of G_i) were consistent with those of σ_F^2 (Fig. 9e, g). The values of $2\overline{V}\sigma_{CG}^2$ (about the mean velocity and the covariance of nutrient concentration and the G_i) were small throughout the Section YE, and their contribution to σ_F^2 was negligible (Fig. 9f).

Because $\overline{C}^2\sigma_V^2$ was determined by $\overline{C}^2$ and σ_V^2, the spatial distributions of $\overline{C}^2$ and σ_V^2 were responsible for that of $\overline{C}^2\sigma_V^2$ (Fig. 10). The values of $\overline{C}^2$ were highest near the Changjiang Estuary, with values of >200 mmol^2 m^{-6}, and then decreased seaward. This was caused by the input of the DIN-rich Changjiang Diluted Water (Guo et al., 2020a, 2020b; Hou et al., 2021). In the western nearshore area, $\overline{C}^2$ was almost vertically uniform, and the tongue of the high $\overline{C}^2$ region extended seaward at the surface. In the eastern region of Section YE, $\overline{C}^2$ was lower than 50 mmol^2 m^{-6} in the upper water layers, and reached 150 mmol^2 m^{-6} at the bottom. The high

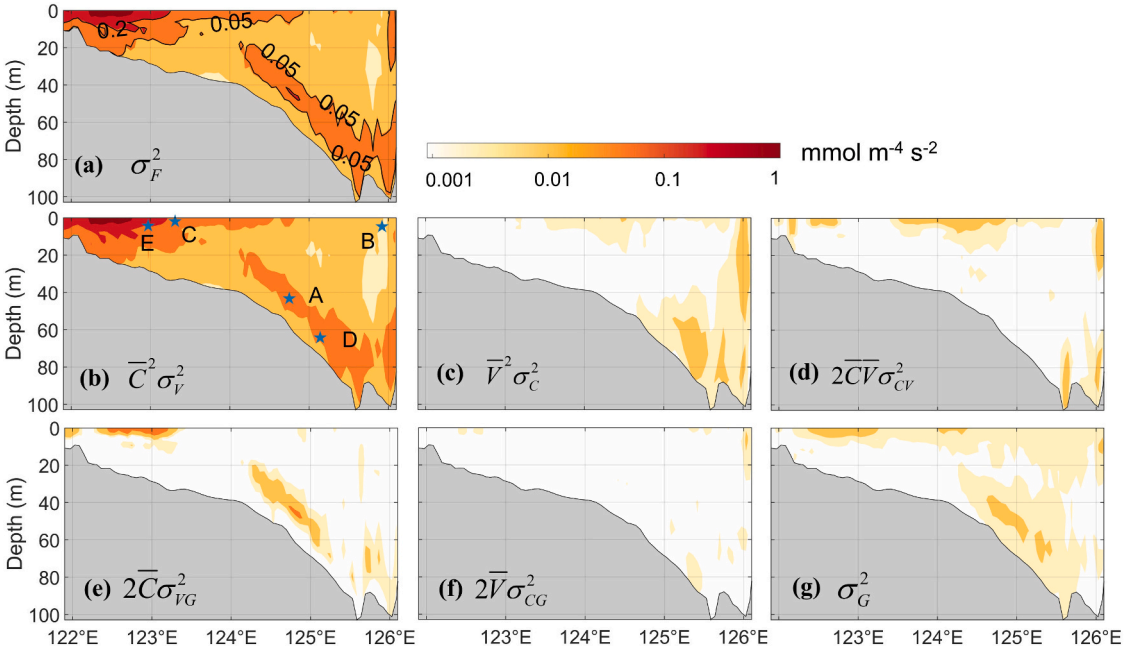

Fig. 9. Spatial distributions of σ_F^2 (a) (unit: mmol m^{-4} s^{-2}) in Eq. (8) and its decomposed items (b–f) at Section YE. The values smaller than 0.001 mmol m^{-4} s^{-2} are shown with the same color. (For interpretation of the references to color in this figure legend, the reader is referred to the web version of this article.)

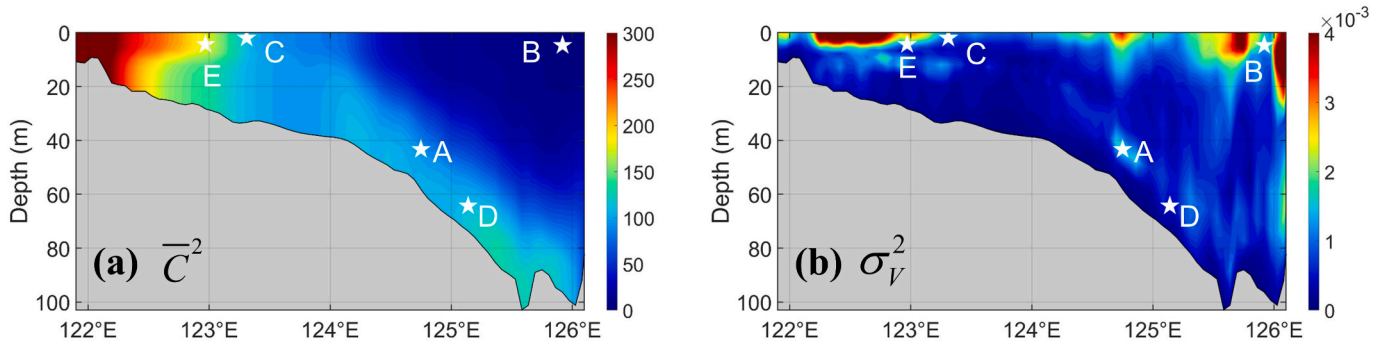

Fig. 10. Vertical distributions of $\overline{C}^2$ (a) (unit: mmol^2 m^{-6}) and σ_V^2 (b) (unit: m^2 s^{-2}) at Section YE. The stars represent the typical sites for studying the influences of $\overline{C}^2$ and σ_V^2 on σ_F^2.

$\overline{C}^2$ band occupied the bottom of the deeper shelf region. σ_V^2 represents the seasonal variations of velocity. A larger value of σ_V^2 indicates stronger seasonal variations in velocity. Areas with larger σ_V^2 values primarily occurred at the surface, with values larger than 3×10^{-3} m^2 s^{-2}. The clear temporal variations in velocity west of 123° E were jointly controlled by Changjiang River discharge and the monsoon. At the surface layer of the deeper region, strong temporal variations in velocity were caused by monsoons and the Cheju Warm Current.

The spatial distributions of $\overline{C}^2$ and σ_V^2 affected those of $\overline{C}^2\sigma_V^2$, and therefore, affected the spatial distributions of σ_F^2. To study the influences of $\overline{C}^2$ and σ_V^2 on σ_F^2, five sites were selected at Section YE (A–E in Fig. 9b), and the values of $\overline{C}^2$, σ_V^2, and σ_F^2 of these five sites were calculated (Table 2). Compared A and B, both had similar values of σ_V^2, indicating there were similar seasonal velocity variations at these two sites. However, $\overline{C}^2$ at A was one order of magnitude larger than that at B. As a result, the seasonal variations of DIN flux at A were significantly stronger than that at B. Compared C and D, $\overline{C}^2$ at C was as high as that at D. However, due to the influence by the Changjiang Diluted Water, seasonal variations of velocity at C were stronger than that at D, which led to the stronger seasonal variations of DIN flux at C. Compared A and E, the annual average of DIN concentration at nearshore E was higher than that at offshore A. However, σ_V^2 at A was larger than that at E. As a result, σ_F^2 at A was similar to σ_F^2 at E, indicating there were similar seasonal variations of DIN fluxes at these two sites. Therefore, the spatial distributions of σ_F^2 were jointly determined by $\overline{C}^2$ and σ_V^2. The most significant seasonal variations of DIN flux usually occurred in the area with large annual average of concentration and strong seasonal variations of velocity.

4.2. Contribution of nutrient exchange across Section YE to the DIN budget of the Yellow Sea

Based on the model result, the annual average DIN fluxes through Section YE and the Cheju Strait were 2.80×10^6 and -1.90×10^6 mmol/s, respectively. Therefore, the net DIN flux through these two southern lateral boundaries of the Yellow Sea was 0.90×10^6 mmol/s, which was consistent with the magnitude calculated in previous researchers (Liu et al., 2003; Zhao et al., 2016). The annual DIN flux through the Bohai Strait was 0.04×10^6 mmol/s. Thus, the annual average DIN flux entering the Yellow Sea through these three lateral boundaries was 0.94×10^6 mmol/s. Near the Changjiang Estuary in Section YE, the annual average DIN input was 0.56×10^6 mmol/s, which represented the DIN flux of the Changjiang River indirectly input into the Yellow Sea through Section YE. The annual average DIN flux from three major rivers of the Yellow Sea (Yalujiang, Han River and Huaihe) was 0.31×10^6 mmol/s, which was approximately half of that indirectly input by the Changjiang River through Section YE. The annual average atmospheric deposition DIN flux was 1.59×10^6 mmol/s, which was comparable to the amount from these three lateral boundaries and only half of that from Section YE. Therefore, among the four external nutrient sources (atmospheric deposition, riverine input, exchange with the Bohai Sea, and exchange with the East China Sea), the DIN from the East China Sea contributed 59 % of the total DIN input. Based on the model, the sources of DIN from the open sea, rivers, and atmospheric deposition were balanced by sinks entering the sediments through net deposition and exchange with the open sea in the form of particulate organic matter.

Table 2
Values of A–E points, $\overline{C}^2$ (unit: mmol^2 m^{-6}), σ_V^2 (unit: m^2 s^{-2}), and σ_F^2 (unit: mmol m^{-4} s^{-2}).

	$\overline{C}^2$	σ_V^2	σ_F^2
A	96.21	1.73×10^{-3}	0.24
B	6.74	1.69×10^{-3}	9.09×10^{-3}
C	113.29	1.24×10^{-3}	0.16
D	112.93	4.56×10^{-4}	5.68×10^{-2}
E	174.61	1.30×10^{-3}	0.25

As shown in Fig. 11, the DIN fluxes from atmospheric deposition and river input were derived from the forcing conditions of the model. Due to the limitations of observation, the atmospheric deposition flux was 1.59×10^6 mmol/s throughout the year, with no seasonal variations. Additionally, the exchange of DIN between the Yellow Sea and adjacent seas exhibited more significant seasonal variations than the DIN from rivers. In winter, the amount of DIN flux from atmospheric deposition was the largest among them, whereas the amount from rivers remained small, and the exchange through lateral boundaries even acted as a sink of DIN for the Yellow Sea. In the other three seasons, net transport across the three lateral boundaries of the Yellow Sea were the source of DIN. Especially in summer, the amount of DIN transported from the adjacent seas reached its maximum value of 2.90×10^6 mmol/s, which was nearly three times the amount transported from the rivers and exceeded the atmosphere. Exchanges of nutrients through sea-sea boundaries play an important role in the nutrient budget and promote primary production in the warm seas of the Yellow Sea.

For the continental East China Sea, DIN exchanged through Section YE was a sink for DIN throughout the year. The continental East China Sea has five lateral boundaries the Section YE, Cheju Strait, an isobath of 200 m in the East China Sea, Tsushima Strait and Taiwan Strait. Among them, the annual average DIN fluxes at the 200 m isobath, Tsushima Strait, and Taiwan Strait were 13.57×10^6, -11.41×10^6, and 1.41×10^6 mmol/s, and the annual DIN flux of exchanging with adjacent sea of East China Sea was 3.20×10^6 mmol/s (Wang et al., 2019). Exchanging with the 200 m isobath was the main source of DIN in the East China Sea, and was caused by the intrusion of the Kuroshio Current into the shelf of the East China Sea, resulting in a DIN flux of 12.6×10^6 mmol/s (Zhang et al., 2019). Exchanging with Tsushima Strait was the main sink of DIN

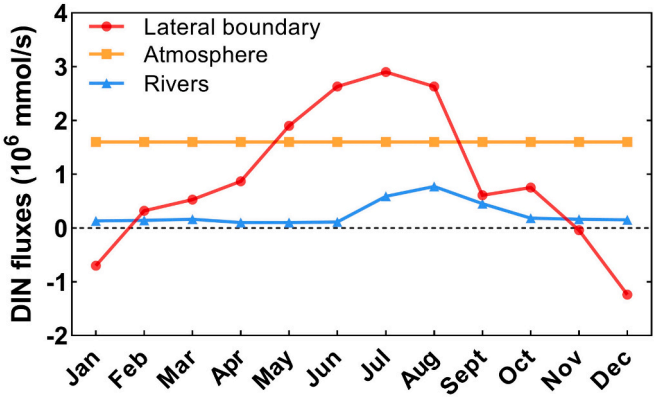

Fig. 11. Seasonal variations of DIN fluxes for external inputs into the Yellow Sea, including lateral boundary, atmosphere, and rivers. A positive value represents DIN flux inflow in the Yellow Sea and a negative value represents DIN flux outflow from the Yellow Sea (unit: 10^6 mmol/s). The red line and circles represent the input from the lateral boundary (the sum of DIN fluxes of Bohai Strait, Cheju Strait, and Section YE); the orange line and squares represent atmospheric deposition; and the blue line and triangles represent riverine input. (For interpretation of the references to color in this figure legend, the reader is referred to the web version of this article.)

in the lateral boundaries of East China Sea, with a DIN flux four times that of the Section YE. However, unlike the Yellow Sea, the influence of Section YE on the East China Sea was comparatively weak. The annual amount of DIN from the atmospheric deposition and rivers were 2.07 × 10^6 and 1.24 × 10^6 mmol/s, both of which were smaller than the amount from the lateral boundaries (Wang et al., 2019). This was indicated that exchange with adjacent seas was the main source of DIN in both the Yellow Sea and East China Sea.

Meanwhile, this study had certain limitations and uncertainties. First, the DIN from various sources were represented by one state variable in our model. Therefore, it needed add a tracking module for nutrients from different origins to describe the path of DIN coming from different source. In addition, the DIN concentrations of atmospheric deposition were collected from 1997 to 2005 with no seasonal variations (Zhang et al., 2011). However, total atmospheric nitrogen deposition has increased in the past few decades (Wang et al., 2020), and seasonal variations of atmospheric deposition can be obtained through air quality models recently (Zhang et al., 2023). Therefore, the atmospheric deposition with high spatiotemporal will be applied in our future research, and the role of exchange across Section YE needs to be evaluated continuously under the changing environmental situations.

5. Conclusions

This study was based on a three-dimensional physical-biogeochemical coupled model and analyzed the seasonal and spatial variations in DIN flux across Section YE. DIN was transported into the Yellow Sea from the East China Sea throughout the year. The inflow of DIN flux in summer was 4.21 × 10^6 mmol/s, which was the largest contributor, accounting for 38 % of the total annual input, while in winter, was the smallest to be 1.71 × 10^6 mmol/s, accounting for 10 % of the DIN input to the Yellow Sea. The northerly monsoon induced the outflow of DIN in the surface layer across Section YE during winter and autumn. The northeastern expansion of the Changjiang Diluted Water resulted in a strong inflow of DIN to the surface layer in the western part of Section YE during summer and spring. The Cheju Warm Current turned clockwise around western Cheju Island throughout the year, resulting in an inflow of DIN in the lower layer of the eastern part of Section YE.

By decomposing the variations in DIN flux, seasonal variations were mainly controlled by seasonal variations in ocean currents, whereas spatial differences in seasonal variations in DIN flux were modulated by the annual average DIN concentration. The DIN flux input to the Yellow Sea through the lateral boundaries (Bohai Strait, Cheju Strait, and Section YE) was higher than that from the direct riverine input and was the same in magnitude as atmospheric deposition. The input from lateral boundaries was an important source of DIN in the Yellow Sea, particularly in summer, when it was the largest source of nutrients.

CRediT authorship contribution statement

Yujun Liu: Writing – original draft, Visualization, Validation, Software, Methodology, Investigation, Formal analysis, Data curation, Conceptualization. **Xinyan Mao:** Validation, Methodology, Investigation. **Jie Shi:** Writing – review & editing, Supervision, Software, Resources, Project administration, Methodology, Investigation, Conceptualization. **Yifei Luo:** Visualization, Validation, Methodology, Investigation, Conceptualization. **Xinyu Guo:** Writing – review & editing, Supervision, Methodology, Formal analysis. **Yucheng Wang:** Methodology.

Declaration of competing interest

The authors declare that they have no known competing financial interests or personal relationships that could have appeared to influence the work reported in this paper.

Data availability

No data was used for the research described in the article.

Acknowledgments

This study was supported by the National Natural Science Foundation of China (no. 42176022, no. 42141017) and the National Key Research and Development Program of China (no. 2023YFF0805001). Y. Liu was supported by the Ministry of Education, Culture, Sports, Science and Technology, Japan (MEXT) to a project on Joint Usage/Research Center–Leading Academia in Marine and Environment Pollution Research (LaMer).

References

Bai, X., Hu, D., 2004. A numerical study on seasonal variations of the Taiwan Warm Current. Chin. J. Oceanol. Limnol. 22, 278–285. https://doi.org/10.1007/BF02842560.

Blumberg, A.F., Mellor, G.L., 1987. A description of a three-dimensional coastal ocean circulation model. In: Heaps, N.S. (Ed.), Three-dimensional Coastal Ocean Models, vol. 4. American Geophysical Union, pp. 1–16. https://doi.org/10.1029/co004p0001.

Chang, P.H., Isobe, A., 2003. A numerical study on the Changjiang diluted water in the Yellow and East China Seas. J. Geophys. Res. 108 (C9), 3299. https://doi.org/10.1029/2002JC001749.

Chang, K.I., Suk, M.S., Pang, I.C., Teague, W.J., 2000. Observations of the Cheju Current. J. Korean Soc. Oceanogr. 3 (35), 129–152.

Dee, D.P., Uppala, S.M., Simmons, A.J., Berrisford, P., Poli, P., Kobayashi, S., et al., 2011. The ERA-Interim reanalysis: configuration and performance of the data assimilation system. Q. J. R. Meteorol. Soc. 137 (656), 553–597. https://doi.org/10.1002/qj.828.

Ding, R., Huang, D., Xuan, J., Zhou, F., Pohlmann, T., 2019. Temporal and spatial variations of cross-shelf nutrient exchange in the East China Sea, as estimated by satellite altimetry and in situ measurements. J. Geophys. Res. Oceans 124 (2), 1331–1356. https://doi.org/10.1029/2018JC014496.

Dong, S., 2019. Researching progresses and prospects in large salmonidae farming in Cold Water Mass of Yellow Sea. Period. Univ. China 49 (3), 1–6. https://doi.org/10.16441/j.cnki.hdxb.20180303.

Fu, M., Wang, Z., Li, Y., Li, R., Sun, P., Wei, X., et al., 2009. Phytoplankton biomass size structure and its regulation in the Southern Yellow Sea (China): seasonal variability. Cont. Shelf Res. 29, 2178–2194. https://doi.org/10.1016/j.csr.2009.08.010Get rights and content.

Gómez, F., 2003. The role of the exchanges through the Strait of Gibraltar on the budget of elements in the Western Mediterranean Sea: consequences of human-induced modifications. Mar. Pollut. Bull. 46 (6), 685–694. https://doi.org/10.1016/S0025-326X(03)00123-1.

Grilli, F., Marini, M., Book, J.W., Campanelli, A., Paschini, E., Russo, A., 2013. Flux of nutrients between the middle and southern Adriatic Sea (Gargano-Split section). Mar. Chem. 153, 1–14. https://doi.org/10.1016/j.marchem.2013.04.005.

Guo, X., Miyazawa, Y., Yamagata, T., 2006. The Kuroshio onshore intrusion along the shelf break of the East China Sea: the origin of the Tsushima warm current. J. Phys. Oceanogr. 36 (12), 2205–2231. https://doi.org/10.1175/jpo2976.1.

Guo, X., Zhu, X.H., Wu, Q.S., Huang, D., 2012. The Kuroshio nutrient stream and its temporal variation in the East China Sea. J. Geophys. Res. Oceans 117, C01026. https://doi.org/10.1029/2011JC007292.

Guo, Y., Rong, Z., Chi, Y., Li, X., Na, R., 2020a. The modeling study of interannual variability of Changjiang River plume in summer season. Trans. Oceanol. Limnol. 4, 30–41. https://doi.org/10.11728/cjss2023.06.2023-0059.

Guo, C., Zhang, G., Sun, J., Leng, X., Xu, W., Wu, C., et al., 2020b. Seasonal responses of nutrient to hydrology and biology in the southern Yellow Sea. Cont. Shelf Res. 206, 104207. https://doi.org/10.1016/j.csr.2020.104207.

Hou, W., Ba, M., Bai, J., Yu, J., 2021. Numerical study on the expansion and variation of Changjiang diluted water in summer and autumn. J. Mar. Sci. Eng. 9, 317. https://doi.org/10.3390/jmse9030317.

Isobe, A., 2008. Recent advances in ocean-circulation research on the Yellow Sea and East China Sea shelves. J. Oceanogr. 64 (4), 569–584. https://doi.org/10.1007/s10872-008-0048-7.

Jiang, H., Zhao, L., Zhang, J., 2020. Budgets and transformation of dissolved inorganic and particulate organic nitrogen in the Yellow Sea: a model study. China Environ. Sci. 40 (9), 3981–3991.

Jin, J., Liu, S.M., Ren, J.L., Liu, C.G., Huang, D.J., 2013. Nutrient dynamics and coupling with phytoplankton species composition during the spring blooms in the Yellow Sea. Deep Sea Res. Top. Stud. Oceanogr. 97, 16–32. https://doi.org/10.1016/j.dsr2.2013.05.002.

Kobayashi, S., Fujiwara, T., 2008. Long-term variability of shelf water intrusion and its influence on hydrographic and biogeochemical properties of the Seto Inland Sea, Japan. J. Oceanogr. 64 (4), 595–603. https://doi.org/10.1007/s10872-008-0050-0.

Li, H., Zhang, C., Han, X., Shi, X., 2015. Changes in concentrations of oxygen, dissolved nitrogen, phosphate, and silicate in the southern Yellow Sea, 1980–2012: sources and seaward gradients. Estuar. Coast. Shelf Sci. 163, 44–55. https://doi.org/10.1016/j.ecss.2014.12.013.

Li, Z., Lin, Q., Li, J., Shan, X., 2019. Present situation and future development of marine ranching construction in China. J. Fish. China 43 (9), 11. https://doi.org/10.11964/jfc.20190311699.

Liang, C., Xian, W., 2018. Changjiang nutrient distribution and transportation and their impacts on the estuary. Cont. Shelf Res. 165, 137–145. https://doi.org/10.1016/j.csr.2018.05.001.

Lie, H., Cho, C., 2016. Seasonal circulation patterns of the Yellow and East China Seas derived from satellite-tracked drifter trajectories and hydrographic observations. Prog. Oceanogr. 146, 121–141. https://doi.org/10.1016/j.pocean.2016.06.004.

Lie, H., Cho, C., Lee, J., Lee, S., Tang, Y., 2000. Seasonal variation of Cheju Warm Current in the northern East China Sea. J. Oceanogr. 56, 197–211.

Liu, S.M., Zhang, J., Chen, S.Z., Chen, H.T., Hong, G.H., Wei, H., et al., 2003. Inventory of nutrient compounds in the Yellow Sea. Cont. Shelf Res. 23 (11–13), 1161–1174. https://doi.org/10.1016/S0278-4343(03)00089-X.

Liu, H., Pang, C., Yang, D., Liu, Z., 2021a. Seasonal variation in material exchange through the Bohai Strait. Cont. Shelf Res. 231, 104599. https://doi.org/10.1016/j.csr.2021.104599.

Liu, Z., Gan, J., Hu, J., Wu, H., Cai, Z., Deng, Y., 2021b. Progress on circulation dynamics in the East China Sea and southern Yellow Sea: origination, pathways, and destinations of shelf currents. Prog. Oceanogr. 193, 102553. https://doi.org/10.1016/j.pocean.2021.102553.

Lu, Z., Gan, J., Dai, M., Zhao, X., Hui, C.R., 2020. Nutrient transport and dynamics in the South China Sea: a modeling study. Prog. Oceanogr. 183, 102308. https://doi.org/10.1016/j.pocean.2020.102308.

Luo, Y., Shi, J., Guo, X., Mao, X., Yao, P., Zhao, B., et al., 2023. Yearly variations in nutrient supply in the East China Sea due to the Zhejiang Coastal Upwelling and Kuroshio Intrusion. J. Geophys. Res. Oceans 128 (4), e2022JC019216. https://doi.org/10.1029/2022JC019216.

Mellor, G., 2003. The three-dimensional current and surface wave equations. J. Phys. Oceanogr. 33 (9), 1978–1989. https://doi.org/10.1175/1520-0485(2003)033<1978:ttcasw>2.0.co;2.

Miyazawa, Y., Zhang, R., Guo, X., Tamura, H., Ambe, D., Lee, J.S., et al., 2009. Water mass variability in the western North Pacific detected in a 15-year eddy resolving ocean reanalysis. J. Oceanogr. 65 (6), 737–756. https://doi.org/10.1007/s10872-009-0063-3.

Naimie, C.E., Blain, C.A., Lynch, D., R., 2001. Seasonal mean circulation in the Yellow Sea — a model-generated climatology. Cont. Shelf Res. 21 (6), 667–695. https://doi.org/10.1016/S0278-4343(00)00102-3.

Onitsuka, G., Yanagi, T., Yoon, J.H., 2007. A numerical study on nutrient sources in the surface layer of the Japan Sea using a coupled physical-ecosystem model. J. Geophys. Res. Oceans 112, C05042. https://doi.org/10.1029/2006JC003981.

Qi, J., Yin, B., Zhang, Q., Yang, D., Chen, H., 2016. Seasonal variation of the volume, heat and salt transport in the East China Sea and adjacent regions. Haiyang Xuebao 38 (11), 1–19. https://doi.org/10.3969/j.issn.0253-4193.2016.11.001.

Shi, Q., 2020. Mechanism and long-term spatio-temporal evolution of hypoxia and anoxia in the South Yellow Sea in summer. J. Appl. Oceanogr. 39 (1), 13. https://doi.org/10.3969/J.ISSN.2095-4972.2020.01.012.

Shi, X., Qi, M., Tang, H., Han, X., 2015. Spatial and temporal nutrient variations in the Yellow Sea and their effects on *Ulva prolifera* blooms. Estuar. Coast. Shelf Sci. 163, 36–43. https://doi.org/10.1016/j.ecss.2015.02.007.

Shibano, R., Morimoto, A., Takayama, K., Takikawa, T., Ito, M., 2019. Response of lower trophic ecosystem in the Japan Sea to horizontal nutrient flux change through the Tsushima Strait. Estuar. Coast. Shelf Sci. 229, 106386. https://doi.org/10.1016/j.ecss.2019.106386.

Shin, C., Min, H.S., Lee, S., Kang, H., Ku, B., Kim, D.G., Park, J., Kwon, S., Choi, B., 2022. Current structure and volume transport in the Jeju Strait observed for a year with multiple ADCP moorings. Ocean Sci. J. 57 (3), 365–380. https://doi.org/10.1007/s12601-022-00079-7.

Skogen, M.D., Søiland, H., 1998. A User's Guide to NORWECOM v2.0. The Norwegian Ecological Model System. Institute of Marine Research.

Sun, S., 2012. New perception of jellyfish bloom in the East China Sea and Yellow Sea. Oceanol. Limnol. Sin. 43 (3), 406–410.

Tak, Y.J, Cho, Y.K, Hwang, J., Kim, Y.Y, 2022. Assessments of Nitrate Budgets in the Yellow Sea Based on a 3D Physical-Biogeochemical Coupled Model. Front. Mar. Sci. 8, 785377. https://doi.org/10.3389/fmars.2021.785377.

Tang, Q., Su, J., Zhang, J., 2010. China GLOBEC II: a case study of the Yellow Sea and East China Sea ecosystem dynamics. Deep Sea Res. II Top. Stud. Oceanogr. 57 (11–12), 993–995. https://doi.org/10.1016/j.dsr2.2008.12.012.

Tang, Q., Ying, Y., Wu, Q., 2016. The biomass yields and management challenges for the Yellow sea large marine ecosystem. Environ. Dev. 17, 175–181. https://doi.org/10.1016/j.envdev.2015.06.012.

Teague, W.J., Jacobs, G.A., Ko, D.S., Tang, T.Y., Suk, M.S., 2003. Connectivity of the Taiwan, Cheju, and Korea straits. Cont. Shelf Res. 23 (1), 63–77. https://doi.org/10.1016/S0278-4343(02)00150-4.

Voss, M., Bange, H.W., Dippner, J.W., Middelburg, J.J., Montoya, J.P., Ward, B., 2013. The marine nitrogen cycle: recent discoveries, uncertainties and the potential relevance of climate change. Philos. Trans. R. Soc. Lond. 368 (1621), 20130121. https://doi.org/10.1098/rstb.2013.0121.

Wang, W., Jiang, W., 2008. Study on the seasonal variation of the suspended sediment distribution and transportation in the East China Seas based on SeaWiFS data. J. Ocean Univ. China 7, 385–392. https://doi.org/10.1007/s11802-008-0385-6.

Wang, B., Shan, B., Zhan, R., Zang, J., 2002. Budget model of inorganic nitrogen in the Bohai and Yellow Sea. Mar. Sci. 26 (2), 33–36.

Wang, J.J., Yu, Z.G., Wei, Q.S., Dong, M.F., Yang, F.X., Li, D.D., et al., 2018. Distributions of nutrients in the western south Yellow Sea in spring and summer of 2017 and their relationship with *UlVa prolifera* outbreaks. Oceanol. Limnol. Sin. 49 (05), 109–117. https://doi.org/10.11693/hyhz20180400086.

Wang, Y., Guo, X., Zhao, L., Zhang, J., 2019. Seasonal variations in nutrients and biogenic particles in the upper and lower layers of East China Sea Shelf and their export to adjacent seas. Prog. Oceanogr. 176, 102138. https://doi.org/10.1016/j.pocean.2019.102138.

Wang, J., Beusen, A.H.W., Liu, X., Van Dingenen, R., Dentener, F., Yao, Q., et al., 2020. Spatially explicit inventory of sources of nitrogen inputs to the Yellow Sea, East China Sea, and South China Sea for the period 1970–2010. Earths Future 8, e2020EF001516. https://doi.org/10.1029/2020EF001516.

Wei, Q.S., Liu, L., Zhan, R., Wei, X.H., Zhang, J.Y., 2010. Distribution features of the chemical parameters in the southern Yellow Sea in summer. Period. Ocean Univ. China 40 (1), 82–88. https://doi.org/10.16441/j.cnki.hdxb.2010.01.014.

Wei, Q., Yu, Z., Wang, B., Fu, M., Xia, C., Liu, L., et al., 2016. Coupling of the spatial–temporal distributions of nutrients and physical conditions in the southern Yellow Sea. J. Mar. Syst. 156, 30–45. https://doi.org/10.1016/j.jmarsys.2015.12.001.

Xuan, J., Zhou, F., Huang, D., Wei, H., Liu, C., Xing, C., 2011. Physical processes and their role on the spatial and temporal variability of the spring phytoplankton bloom in the central Yellow Sea. Acta Ecol. Sin. 31 (1), 61–70. https://doi.org/10.1016/j.chnaes.2010.11.011.

Zhai, F., Liu, Z., Li, P., Gu, Y., Sun, L., Hu, L., et al., 2021. Physical controls of summer variations in bottom layer oxygen concentrations in the coastal hypoxic region off the northeastern Shandong Peninsula in the Yellow Sea. J. Geophys. Res. Oceans 126, e2021JC017299. https://doi.org/10.1029/2021JC017299.

Zhang, J., 1996. Nutrient elements in large Chinese estuaries. Cont. Shelf Res. 16 (8), 1023–1045. https://doi.org/10.1016/0278-4343(95)00055-0.

Zhang, J., Zhang, G.S., Bi, Y.F., Liu, S.M., 2011. Nitrogen species in rainwater and aerosols of the Yellow and East China seas: effects of the East Asian monsoon and anthropogenic emissions and relevance for the NW Pacific Ocean. Glob. Biogeochem. Cycles 25, GB3020. https://doi.org/10.1029/2010GB003896.

Zhang, J., Guo, X., Zhao, L., 2019. Tracing external sources of nutrients in the East China Sea and evaluating their contributions to primary production. Prog. Oceanogr. 176, 102122. https://doi.org/10.1016/j.pocean.2019.102122.

Zhang, J., Liu, X., Wang, J., He, H., Yao, X., Gao, H., 2023. Atmospheric dry deposition fluxes of trace metals over the Eastern China Marginal Seas: impact of emission controls. Sci. Total Environ. 873, 162117. https://doi.org/10.1016/j.scitotenv.2023.162117.

Zhao, L., Guo, X., 2011. Influence of cross-shelf water transport on nutrients and phytoplankton in the East China Sea: a model study. Ocean Sci. 7 (1), 27–43. https://doi.org/10.5194/os-7-27-2011.

Zhao, C., Zang, J., Liu, J., Sun, T., Ran, X., 2016. Distribution and budget of nitrogen and phosphorus and their influence on the ecosystem in the Bohai Sea and Yellow Sea. China Environ. Sci. 36 (07), 2115–2127.

Zhu, J., Shi, J., Guo, X., Gao, H., Yao, X., 2018. Air-sea heat flux control on the Yellow Sea Cold Water Mass intensity and implications for its prediction. Cont. Shelf Res. 152, 14–26. https://doi.org/10.1016/j.csr.2017.10.006.